HAL open science

Femtosecond visible transient absorption spectroscopy of chlorophyll- f -containing photosystem II

Noura Zamzam, Rafal Rakowski, Marius Kaucikas, Gabriel Dorlhiac, Sefania Viola, Dennis Nürnberg, Andrea Fantuzzi, A. William Rutherford, Jasper van Thor

To cite this version:

Noura Zamzam, Rafal Rakowski, Marius Kaucikas, Gabriel Dorlhiac, Sefania Viola, et al.. Femtosecond visible transient absorption spectroscopy of chlorophyll- f -containing photosystem II. Proceedings of the National Academy of Sciences of the United States of America, 2020, 117 (37), pp.23158-23164. 10.1073/pnas.2006016117 . hal-04004130

HAL Id: hal-04004130

https://amu.hal.science/hal-04004130v1

Submitted on 23 Mar 2023

HAL is a multi-disciplinary open access archive for the deposit and dissemination of scientific research documents, whether they are published or not. The documents may come from teaching and research institutions in France or abroad, or from public or private research centers.

L'archive ouverte pluridisciplinaire **HAL**, est destinée au dépôt et à la diffusion de documents scientifiques de niveau recherche, publiés ou non, émanant des établissements d'enseignement et de recherche français ou étrangers, des laboratoires publics ou privés.

Distributed under a Creative Commons Attribution 4.0 International License

Main Manuscript for

Femtosecond visible transient absorption spectroscopy of chlorophyll *f*-containing Photosystem II

Noura Zamzam[a], Rafal Rakowski[a], Marius Kaucikas[a], Gabriel Dorlhiac[a,1], Sefania Viola[a], Dennis J. Nürnberg[a,b], Andrea Fantuzzi[a], A. William Rutherford[a], and Jasper J. van Thor[a,*]

[a]Department of Life Sciences, Imperial College London, London, UK

[b]Institute of Experimental Physics, Freie Universität Berlin, Berlin, Germany

[1]Current address: Biophysics Group, University of California Berkeley, Berkeley, California, USA

*To whom correspondence may be addressed: Jasper J. van Thor

Email: j.vanthor@imperial.ac.uk

Classification

Physical Sciences: Biophysics

Keywords

ultrafast | photosynthesis | far-red light | energy transfer | charge separation

Author Contributions

J.J.v.T. and A.W.R. designed research; M.K., R.R., and N.Z. performed measurements; D.J.N. and S.V. prepared samples and edited the manuscript; M.K., G.D., and N.Z. analysed data; N.Z., M.K., A.W.R., A.F and J.J.v.T. wrote the manuscript.

Abstract

The recently discovered, chlorophyll-*f* containing, far-red Photosystem II (FR-PSII) supports far-red light photosynthesis. The participation and kinetics of spectrally shifted far-red pigments are directly observable and separated from that of bulk chlorophyll-*a*. We present an ultrafast transient absorption study of FR-PSII, investigating energy transfer and charge separation processes. The results show a rapid sub-picosecond energy transfer from chlorophyll-*a* to the long-wavelength chlorophylls-*f/d*. The data demonstrate the decay of a ~720 nm negative feature on the picosecond to nanosecond timescales, coinciding with charge separation, secondary electron transfer and stimulated emission decay. A ~675 nm bleach attributed to the loss of chl-*a* absorption due to the formation of a cation radical, $P_{D1}^{+\bullet}$, is only fully developed in the nanosecond spectra, indicating an unusually delayed formation. A major spectral feature on the nanosecond timescale at 725 nm is attributed to an electrochromic blue-shift of a FR-chlorophyll among the reaction centre pigments. These time-resolved observations provide direct experimental support for the model of Nürnberg et al. (2018, *Science* 360, 1210–1213), in which the primary electron donor is a FR-chlorophyll and the secondary donor is chlorophyll-*a* (P_{D1} of the central chlorophyll pair). Efficient charge separation also occurs using selective excitation of long-wavelength chlorophylls-*f/d*, and the localisation of the excited state on P_{720}* points to a smaller (entropic) energy loss compared to conventional PSII, where the excited state is shared over all the chlorin pigments. This has important repercussions on understanding the overall energetics of excitation energy transfer and charge separation reactions in FR-PSII.

Significance Statement

Far-red Photosystem II (FR-PSII) contains a small number of FR-chlorophylls (-*f* or -*d*) with the rest (~85%) being chlorophyll-*a* molecules. Here ultrafast studies on FR-PSII

support a model in which the primary electron donor is a FR-chlorophyll (P_{720}, likely in the Chl_{D1} position), while the second electron donor is chlorophyll-*a* at the P_{D1} position, forming $P_{D1}^{+\bullet}$. Excitation energy transfer from chlorophyll-*a* to the FR-chlorophylls is ultrafast. The excited state of FR-chlorophyll remains highly localised, i.e. P_{720}* does not share the excitation with the chlorophyll-*a* pigments. This is markedly different from both the conventional, chlorophyll-*a* PSII and the chlorophyll-*d* PSII of *Acaryochloris marina*. The entropic and site-energy differences result in efficient but apparently slower stabilisation of the charge-separated state.

Main Text

Introduction

Photosystem II (PSII) is a pigment-protein complex found in plants, algae and cyanobacteria. It plays a major role in photosynthesis as the water/plastoquinone photooxidoreductase, responsible for the water-splitting reaction that puts oxygen into the atmosphere (1). The structure and function of PSII have been extensively investigated using a wide range of methods including X-ray crystallography (2–6). PSII is made up of a central pair of near-symmetrical protein subunits, D1 and D2, containing the cofactors involved in photochemical charge separation, water oxidation and quinone reduction. The central D1/D2 subunits are surrounded by the CP43 and CP47 antenna subunits (2–6). Excitation by light of a chlorophyll in PSII is shared between the chlorophylls and the pheophytins through excitation transfer. When a redox active chlorophyll in the D1/D2 reaction centre is excited, charge separation occurs. The central reaction centre chlorin pigments, which are collectively known as P680, are made up of four chlorophyll-*a* (chl-*a*) molecules, P_{D1}, P_{D2}, Chl_{D1}, Chl_{D2} and two pheophytin-*a* molecules ($Pheo_{D1}$ and $Pheo_{D2}$). The order and timing of charge separation and electron transfer remains rather uncertain despite extensive research (2–4).

Several lines of evidence, including ultrafast kinetic studies, indicate that charge separation proceeds at least in part via the formation of $Chl_{D1}^{+\bullet}Pheo_{D1}^{-\bullet}$ as the first radical pair (RP1) (3, 4, 7–12). It is also thought RP1 could be a distribution of $Chl_{D1}^{+\bullet}Pheo_{D1}^{-\bullet}$ in some centres and $P_{D1}^{+\bullet}Chl_{D1}^{-\bullet}$ in others (13, 14). However, the view that RP1 in PSII is $P_{D1}^{+\bullet}Chl_{D1}^{-\bullet}$ in all the centres is still advocated (15). This model was originally based on the photochemistry in the well-characterised purple bacterial reaction centre, where RP1 is $P^{+}B^{-}$, P is a special pair of (bacterio)chlorophylls over which the cation is shared and B is a monomeric (bacterio)chlorophyll (16). Irrespective of the identity of RP1, the secondary radical pair (RP2) in PSII is thought to be $P_{D1}^{+\bullet}Pheo_{D1}^{-\bullet}$. The electron transfer from $Pheo_{D1}^{-\bullet}$ to $Q_{A,}$ leads to formation of $P_{D1}^{+\bullet}Q_{A}^{-\bullet,}$ RP3 (2–4, 9, 15). This uncertainty in the order and timing of the charge separation process is compounded by uncertainty over the rates and reversibility of excitation energy transfer (17).

These difficulties arise in large part from the fact that all the 37 chlorins in PSII cores (35 chlorophylls-*a* and 2 pheophytins-*a*) are essentially the same colour. This means i) there is little scope for wavelength selectivity, ii) spectral deconvolution is near-intractable, iii) there is little driving force for directionality of excitation energy transfer, and consequently, iv) excitation is shared over all the pigments.

In 2010, a new form of chlorophyll was discovered in cyanobacteria: chlorophyll-*f* (chl-*f*) (18). Chl-*f* differs from chl-*a* chemically through the substitution of the methyl group at the C-2 position by a formyl group, causing the Q_y absorption band to shift to significantly longer wavelengths, e.g. from 670 nm to 706 nm in methanol (18). This pigment is synthesised when some species of cyanobacteria grow in environments where most of the visible spectrum is shaded but far-red and near-infrared light is abundant. Under these conditions a variant form of PSII is expressed (19). In the case of *Chroococcidiopsis thermalis* PCC 7203, this far-red PSII (FR-PSII) contains 4 chl-*f*, 1 chl-*d* and ~30 chl-*a* and the long-wavelength chlorophylls were shown not only to be antenna pigments, but also to be responsible for primary charge separation (12).

Similar rates of PSII activity measured for FR-PSII excited with visible and far-red light at both room temperature and cryogenic temperatures showed that a far-red light chlorophyll, either chl-*f* or chl-*d*, was the primary electron donor (12). In the light-minus-dark 77 K difference absorption spectrum, a blue-shift centred at 727 nm was attributed to long-wavelength Chl_{D1}, because, in conventional, chlorophyll-*a*-containing PSII, Chl_{D1} gives rise to the dominant blue-shift (~680 nm) upon $Q_{A}^{-\bullet}$ formation. A similar shift was seen when $Pheo_{D1}^{-\bullet}$ was formed. These observations suggested that Chl_{D1} is the long-wavelength chlorophyll in FR-PSII that acts as the primary donor. This was supported by

the finding that FR-PSII is highly luminescent, suggesting a smaller energy gap between P* (the excited state of the primary donor) and the primary radical pair (RP1), consistent with a long-wavelength primary donor (12).

Fitting of the 1.8 K magnetic circular dichroism (MCD) and absorption spectra of isolated FR-PSII indicated five long-wavelength chlorophylls with absorption maxima at 721, 727, 734, 737, and 749 nm. The primary donor, giving rise to the 727 nm band shift and suggested to be Chl_{D1}, could not be definitively assigned to either chl-*d* or chl-*f* but chl-*f* was considered the more likely candidate (12).

The presence of 5 FR-chlorophylls, which were not only shifted from the bulk absorption of chlorophyll-*a* but also distinguishable from each other, provides a unique opportunity to resolve the primary events in PSII (12). This unprecedented alleviation of the spectral congestion that has complicated spectral and mechanistic assignments in PSII research, makes FR-PSII particularly attractive for a range of spectroscopic studies. In addition to understanding the novel FR-PSII itself, these studies could provide insights relevant to conventional chl-*a* PSII. The only previous sub-nanosecond time-resolved studies of FR-PSII used time-correlated single-photon counting fluorescence measurements in far-red light grown intact cells of *Halomicronema hongdechloris* (20, 21). Here we report a femtosecond to nanosecond visible transient absorption study of energy transfer and charge separation kinetics from what is at present, the only published preparation of isolated FR-PSII cores (12). This material was isolated from FR-grown *C. thermalis* and has been the subject of detailed biochemical and biophysical analyses (12).

Results

Transient absorption measurements were performed with two types of PSII core complexes: i) from *C. thermalis* grown under far-red light conditions, FR-PSII, and ii) from *Thermosynechococcus elongatus* grown in white light, WL-PSII. The experimental data for the WL-PSII, which are shown and described in detail in the SI Appendix, were similar to those reported in the literature.

Transient absorption spectra and lifetime maps of FR-PSII

The FR-PSII spectra were obtained for two excitation wavelengths, 675 nm and 720 nm. The 675 nm excitation is absorbed primarily by the chl-*a* pigments (Fig. 1a), whereas 720 nm excitation is absorbed only by the long wavelength pigments, chl-*f* and chl-*d* (Fig. 1b). The transient absorption spectra at selected delays for both excitation wavelengths

are shown in panels a and b of Fig. 1. Panels c and d of Fig. 1 show the corresponding lifetime density maps.

Close to time zero, the 675 nm excitation resulted in a difference spectrum showing one major negative feature at 677 nm attributed to i) a ground state bleach (GSB) of chlorophyll-*a* and ii) stimulated emission (SE) band. In addition, an excited state absorption (ESA) at 655 nm and broadband absorption in the 500-650 nm region (Fig. 1a black spectrum) are evident. Those features are quite similar to those seen in WL-PSII (SI Appendix, Fig. S2), except that the FR-PSII spectrum also shows a small GSB/SE band at 705 nm, the short-wavelength edge of the FR-chlorophyll absorption.

In the 0.25 ps difference spectrum (Fig. 1a), the minor GSB/SE band at ~705 nm increased in amplitude and its peak shifted by 4 nm to 709 nm. The amplitude of the main GSB/SE band at 677 nm also increased in this spectrum. In contrast, the 0.5 ps spectrum shows a decrease in the amplitude of the main GSB/SE band, while the amplitude of the 709 nm GSB/SE band continued to increase.

In the 1 ps spectrum, the GSB/SE band at ~677 nm decreased further, while the 712 nm GSB/SE band increased further dominating the spectrum. By 10 ps, the GSB/SE in the 670-680 nm region had completely decayed, leaving a positive band at 656 nm and a major GSB/SE band at 720 nm as the main features in the spectrum (Fig. 1a).

At 100 ps, the amplitudes of the positive band at 656 nm and the ~720 nm GSB/SE decreased, the latter shifting further to the red, 722 nm. In the 2000 ps spectrum, the long-wavelength feature is at 727 nm and a small GSB at 675 nm is present (Fig. 1a).

The lifetime density maps shown in Fig. 1 (panels c and d) are the result of lifetime density analysis performed on the TA data using a semi-continuous distribution of ~100 lifetimes in the 100 fs - 10 ns range (22). The maps provide a model-free analysis of the wavelength dependence of the TA kinetics with a choice of regularization technique that is particularly well-suited to the highly heterogenous photosynthetic dynamics (22). The lifetime density map in Fig. 1c transforms the full dataset generated with 675 nm excitation of FR-PSII. The features described in the transient absorption spectra (Fig. 1a) are reflected in the maps. Interestingly, a second positive feature at 2-3 ps can be noted in the 660-670 nm region in addition to the positive peak in the 720-740 nm region that correspond to the bleach and stimulated emission in the transient absorption spectrum. This feature indicates a decay in the excited state absorption in the region, which could be due to an early charge separation.

The lifetime density map in Fig. 1c also shows two positive peaks centred at 670 nm, one at 60 ps, the other at 1000 ps. These could reflect the lifetimes associated with the appearance of the 675 nm GSB in the long delay spectrum. The discontinuities in the 10 ps and 100 ps spectra (Fig. 1a) at ~670 nm could reflect the early onset of the 675 nm bleach.

Fig. 1b shows transient absorption spectra of FR-PSII using 720 nm excitation. Compared to the data with 675 nm excitation, there is much less spectral evolution. The initial negative feature (GSB/SE) at 713 nm and the positive peak at 660-663 nm dominate the spectrum at delays close to time zero. There is also broadband absorption in the 500-650 nm region (Figs. 1b, d).

There are no major modifications in the spectra at 1 ps and 10 ps apart from a small change in the shape of the features. In the 100 ps spectrum, a shift of the main GSB/SE band to 717 nm is seen. The spectrum at 2000 ps delay is very similar to that observed for 675 nm excitation and consists of two negative features, the more intense one at 725 nm and a smaller one at 675 nm (Fig. 1b).

Consequently, the TA data collected with 720 nm excitation produced a much simpler lifetime map (Fig. 1d). The major GSB/SE band is reflected in a positive peak appearing around 715 nm on a sub-picosecond scale in the lifetime density map (Fig. 1d). There are three distinct negative peaks with approximately 0.7 ps, 20 ps and 400 ps time-constants in the same wavelength region. The positive peak seen at ~670 nm at ~1000 ps in the lifetime density map with 720 nm excitation (Fig. 1d), appears to correspond to a similar peak at ~670 nm with a similar lifetime when 675 nm excitation was used (Fig. 1c).

Fig. 2 shows the transient absorption spectra of FR-PSII at 2 ns and 12 ns delays. It is expected that contributions arising from stimulated emission should greatly decrease or fully decay at the longer times. Comparing the 2 ns and 12 ns spectra, both negative features at 675 nm and 725 nm are still present in the 12 ns spectrum despite the decay in the 725 nm band. The presence of both bands at 12 ns indicates that they both are associated with the charge-separated state, presumably RP3, $P_{D1}^{+\bullet}Q_A^{-\bullet}$. The spectra appear to be similar for both excitation wavelengths, but with 675 nm excitation resulting in a larger amplitude presumably due to its much bigger absorption cross section compared to that at 720 nm.

The 12 ns spectra show significant decrease in the positive peak in the 650 nm region and thus, the state responsible for it had largely decayed by this time-point. This observation supports the assignment of the positive 655 nm band in long delay spectra to excited state absorption. The excited state absorption that decayed in this time window corresponds to the decay of the stimulated emission at 725 nm (Fig. 2).

Furthermore, the position of the 675 nm bleach in the 12 ns spectrum with 675 nm excitation (Fig. 2, left) is slightly blue-shifted relative to the 2 ns delay measurement. This could be a result of the decayed overlapping positive peak or an electrochromic effect. However, it should be noted that due to the long delay introduced in the probe optical path, the precision of wavelength calibration in the 12 ns data is lower than in the data obtained at shorter delays.

TA spectra were also obtained at 27 ns, a time where the fluorescence should be virtually absent (SI Appendix, Fig. S5). The spectra were similar to the 12 ns spectra but with further decay of the 725 nm band, indicating a contribution from stimulated emission even at 12 ns. A residual stimulated emission contribution from chl-*f* at 12 ns is also inferred from the presence of the negative feature at 725 nm when the sample translator was switched off, i.e. with closed centres (SI Appendix, Fig. S8).

Comparison of the raw transient absorption data of WL-PSII (SI Appendix, Fig. S2) and FR-PSII at 675 nm excitation (Fig. 1a) shows that the FR-PSII spectra are only similar to those of WL-PSII at very early delays. Within the first 10 ps, the dominant feature in WL-PSII data, the GSB/SE at 675 nm , is fully replaced by the GSB/SE at 720 nm in FR-PSII. It is clear that most of the excitation energy is transferred from chl-*a* pigments to chl-*f/d* on the 10 ps timescale.

The improved spectral resolution of FR-PSII due to distinct absorption features of the FR-chlorophyll playing antenna and redox roles allows the spectral evolution of distinct bands to be followed providing easier assignments of charge-separated states compared with the WL-PSII spectra.

Homogeneous modelling

Although a homogeneous (sequential) modelling of the TA datasets does not reflect the complex dynamics of the excitation energy transfer and charge separation in PSII cores, it can provide useful insights and inform more sophisticated models. The resulting compartments that represent the discrete set of time-constants that describe the data will have heterogeneous contributions, but the separation is based on the statistical

significance of the amplitudes of the spectral dynamics. The aim is therefore to analyse the spectra that replace each other sequentially in time. Thus, sequential compartment models were applied to both WL- and FR-PSII data, with the number of compartments chosen using Singular Value Decomposition (23) and the correspondence of the resulting time-constants to the lifetime maps. The homogeneous model for the WL-PSII 675 nm excitation data is presented in the SI Appendix, Fig. S4, while those for FR-PSII are shown in Fig. 3. The resulting time-constants are also shown in the lifetime maps in Fig. 1c and d.

Figure 3a shows the globally fitted homogeneous spectra obtained for the TA data of FR-PSII with 675 nm excitation using five compartments. The spectrum in compartment A with a time-constant of 0.5 ps has similar features as the equivalent spectrum in the WL-PSII sequential fit (SI Appendix, Fig. S4): a major GSB/SE band around 677 nm, excited state absorption around 640 nm, broad absorption in the 500-650 nm region and around 780 nm, and stimulated emission around 740 nm. The spectrum is thus dominated by features attributed to the formation of excited state chl-*a* antenna.

The compartment B spectrum, with a time-constant of 3.4 ps, shows significant changes: the main GSB/SE band around 677 nm in the compartment A spectrum decreased in B and was replaced by GSB/SE at 712 nm indicating a loss of Q_y ground state absorption of a far-red chlorophyll. This change of the major GSB/SE band position is attributed to the transfer of excitation energy from chl-*a* antenna to chl-*f/d*. The transition occurring from compartment A to B is rapid, with a sub-picosecond time-constant indicating that the chl-*f/d* pigments involved are close to the excited chl-*a* pigments. The chl-*f/d* bleached at short times are thus likely to be part of the antenna of PSII core complex, perhaps a linker between the chl-*a* pigments and the other longer wavelength chlorophylls including the photochemical trap, as suggested earlier (12). This rapid downhill energy transfer process is kinetically comparable to other downhill light-harvesting processes in the literature in purple bacterial antenna (e.g. (24)), plant LHCII (25) and most pertinently from chl-*a* to chl-*f* in FR-PSI (26, 27).

In the spectrum of compartment C (with a 56 ps time-constant), the GSB/SE in the 670-680 nm region seen in the earlier compartments, which was initially indicative of the presence of excited state chl-*a*, had fully decayed. The spectrum is dominated by a chl-*f/d* GSB/SE at 719 nm, and a positive band at 657 nm (Fig. 3a). The positive band at 657 nm may represent broad excited state absorption of the long-wavelength chlorophyll (see below). At this point all excitation energy has been transferred to FR pigments. The 56 ps time-constant is close to the 50 ps time-constant observed in WL-PSII data (SI Appendix,

Fig. S4). A slight decrease in the broad excited state absorption around 500 nm, compared to that in compartments A and B, may indicate radical-pair formation. Thus, the compartment C spectrum may reflect the formation of the charge-separated state (RP1).The negative feature at 720 nm clearly arises from the long-wavelength chlorophyll, but it could contain contributions from the loss of ground state absorption due to the presence of excited state and/or cation state as well as from stimulated emission (see below).

The spectrum of the next compartment, D (720 ps), is similar to that of compartment C, except the negative band is further shifted to 723 nm and there is a reduction of all band amplitudes. At such a long delay (720 ps), charge separation would have occurred in WL-PSII (8, 9, 17, 28–30) and thus might be expected in FR-PSII. There is a small feature around 675 nm, which could be caused by a decrease of the ground state absorption of chlorophyll-*a* and/or pheophytin due to formation of a chlorophyll-*a* cation radical ($P_{D1}^{+\bullet}$) and/or the expected pheophytin anion radical ($Pheo_{D1}^{-\bullet}$). However, given the small size of the 675 nm bleach, if there is a contribution from a chl-*a* cation (e.g. $P_{D1}^{+\bullet}$ see below), it is not yet fully formed.

Compartments C and D, with time-constants of 56 ps and 720 ps, are both much shorter than the fluorescence lifetime (a few ns) of the isolated chl-*f/d* pigment (31); thus, the events occurring in these lifetimes are likely to be steps in energy transfer and charge separation rather than radiative decay of the excitation energy.

In the spectrum of compartment E, the 675 nm bleach reaches its full amplitude and the long wavelength band is further shifted to 725 nm (Fig. 3a). A small but noticeable broad absorption around 775 nm present in this compartment spectrum is tentatively attributed to a chlorophyll cation. It is similar to the broadband absorption beyond 700 nm observed in WL-PSII spectra (SI Appendix, Fig. S4). In WL-PSII, the radical pair formed at this time is RP3, $P_{D1}^{+\bullet}Q_A^{-\bullet}$, which is stable on the nanosecond timescale. While other assignments of the two negative features are possible (e.g.: loss of chl-*f/d* and chl-*a* ground state absorptions due to formation of chl-$f/d^{+\bullet}$ in equilibrium with a chl-$a^{+\bullet}$, or loss of chl-*f/d* ground state absorption due to formation of a chl-$f/d^{+\bullet}$ in addition to an electrochromic shift on a chl-*a*), we favour the conventional assignment of the final radical pair state to $P_{D1}^{+\bullet}Q_A^{-\bullet}$, with the 675 nm bleach attributed to the formation of $P_{D1}^{+\bullet}$ and the 725 nm feature to an electrochromic blue-shift caused by the charges on $P_{D1}^{+\bullet}Q_A^{-\bullet}$. This fits with the report of an electrochromic blue-shift of a 727 nm chlorophyll due to the charge on $Q_A^{-\bullet}$ formed at cryogenic temperatures (12). Our assignment also fits with

the model of Nürnberg *et al.* (12), in which a chl-*f/d* acts as the primary donor (in the Chl_{D1} location) and a chl-*a* in the P_{D1} position acts as the secondary donor.

When 720 nm excitation is used, the sequential fit results are much less complex than with 675 nm excitation, and a three-compartment model is sufficient to describe the data (Fig. 3b). The spectra of the three compartments (A, B and C) using 720 nm excitation are very similar to those of compartments C, D and E in the 675 nm excitation sequential fit. It seems clear that the reactions occurring are the same except for the transfer of excitation from chl-*a* antenna to chl-*f*, which occurs when chl-*a* is excited by 675 nm light.

The expected Pheo Q_x bleach around 546 nm is not evident in the ultrafast FR-PSII spectra (Fig. 3) but a Pheo Q_x bandshift does appear to be present in the nanosecond spectra (Fig. 2). Its presence fits with the reports of 2 pheophytin-a molecules per PSII and the $Q_A^{-\bullet}$-induced bandshift from the $Pheo_{D1}$ Q_x band at 546 nm in the low temperature absorption difference spectra (12). This shows that in FR-PSII, the $Pheo_{D1}$ occupies its usual position and thus likely plays its usual role as the primary electron acceptor. The absence of clear changes from $Pheo^{-\bullet}$ in the Q_x region at 546 nm and only weak bleaching in the Q_y region at ~670 nm in the ultrafast kinetics (in the 10 ps and 100 ps spectra in Fig. 1a as pointed out earlier) might be explained by a change in the kinetics of its formation and/or decay. This could occur if electron transfer to Pheo were slower or if the rate of transfer from $Pheo^{-\bullet}$ to Q_A were faster. The ~546 nm spectral feature in the nanosecond spectra suggests the former possibility (Fig. 2).

Discussion

The transient absorption spectra presented here provide a number of clear insights into primary charge separation in FR-PSII. These insights rely on the unprecedented spectral resolution intrinsic to this recently discovered system.

<u>Excitation energy transfer from chl-*a** to chl-*f/d*.</u>

Comparisons of the FR-PSII spectra obtained by exciting chl-*a* (675 nm) with those obtained when directly exciting chl-*f/d* (720 nm) show marked differences that are

straightforward to interpret. The pigment bleaching associated with the formation of chl-*a** in the antenna is followed by the ultrafast transfer of the excitation energy to the chl-*f/d*. This occurs on the sub-picosecond to a few picoseconds timescale. Once that has occurred, the evolution of the spectra in time matches what occurs when chl-*f/d* is excited directly using 720 nm light.

When the long-wavelength chlorophylls are excited, either directly or from excitation energy transfer from chl-*a*, the excitation remains localized on the chl-*f/d* without redistributing back to the chlorophylls-*a*. Given the energy difference between chl-*a* and the long wavelength chlorophylls (~40 nm ≈ 100 meV), this is understandable, but the possibility existed that the two sets of pigments were closely interacting or were tuned to span the energy gap and thus would have allowed back-transfer. This does not appear to occur, which fits with the distribution of wavelengths for the far-red chlorophylls reported earlier (12).

The evolution of the long-wavelength feature in time consists of a shift to longer wavelengths: from 705 nm to 727 nm after downhill excitation transfer from chl-*a** (with 675 nm excitation), and from 713 nm to 725 nm when excitation was directly into chl-*f/d* (with 720 nm excitation). The shortest wavelengths (705-709 nm) are associated with the fastest transfer. Nevertheless, at later times (1 ps; Fig. 1a) the band position is still at a relatively short wavelength, 712 nm, but with time it moves to longer wavelengths, ending up at about ~725 nm (in the nanosecond spectra; Fig. 2).

The ~712 nm GSB/SE band may reflect the excitation on the chl-*f/d* that has the shortest wavelength. Fittings of the absorption spectra at 1.8 K indicated that there is only one long-wavelength chlorophyll with an absorption maximum at a shorter wavelength than the electrochromically shifted chl-*f/d* in the presence of $Q_A^{-\bullet}$ and $Pheo^{-\bullet}$(12). The electrochromically shifted chlorophyll was attributed to the primary electron donor, while the far-red pigment with the shortest wavelength was suggested to be the chl-*d*, because of its intrinsic absorption properties. The shortest wavelength chlorophyll of the 5 chlorophylls-*f/d* was suggested to have a role as a “linker” pigment, acting as a physical and energetic bridge between the other 4 long-wavelength chlorophylls and the chl-*a* and/or the allophycocyanin antenna (12). The present data are consistent with such a role.

We note the absorption peak positions for the long-wavelength chlorophylls at 1.8 K appeared to be shifted further to long wavelengths (by ~7 nm) compared to their positions at room temperature (12). The current study, which is done at room temperature, appears to fit with the previous room temperature position for the bandshift at 720 nm. The

discussion of this feature and the proposed linker chlorophyll *f/d* at ~712 nm, takes this temperature-induced shift into account when comparing with the 1.8 K spectra.

Excited state decay.

The spectra collected on the few to tens of nanoseconds timescale showed a decrease in the long-wavelength negative feature. Light emission from an excited state chlorophyll will be detected as stimulated emission in the wavelength range of spontaneous fluorescence. Chlorophyll fluorescence in photosynthesis is expected to decay in ~5 ns (32). It is thus likely that some of the reduction in the amplitude of the negative feature at 725 nm is associated with the decay of stimulated emission from the excited state of the long-wavelength chlorophyll contributing to the feature. This could reflect a small fraction of centres that are closed (where $Q_A^{-\bullet}$ is present before the flash), although tests showed that the centres were primarily open (see SI Appendix). In order to ensure that excited state decay was complete, additional measurements with an even longer delay time of 27 ns were made, and this spectrum still exhibited the negative feature at 725 nm. This confirmed its assignment to a feature associated with the final radical pair state.

Charge separation.

The spectral evolution of the long-wavelength features at both excitation wavelengths (675 nm and 720 nm) demonstrate the direct involvement of chlorophyll-*f* in the primary charge separation reactions, a view that was recently proposed (12) and that challenged the original consensus that chlorophyll-*f* only functions as an antenna pigment (33).

The spectra taken at the longest times and attributed to $P_{D1}^{+\bullet}Q_A^{-\bullet}$, contain two negative features at 675 nm and 725 nm. In the context of the existing model, these are assigned to the loss of ground state absorption of chl-*a* at 675 nm due to the formation of the cation radical $P_{D1}^{+\bullet}$, and to the long wavelength trough (725 nm) of an electrochromic shift on the absorption of a FR-chlorophyll centred at 720 nm and proposed to be Chl_{D1} (12).

The model proposes that the FR-Chl_{D1} is the primary donor, while a chl-*a* P_{D1} is the secondary donor and bearer of the final chlorophyll cation radical. The kinetic measurements are consistent with this model.

The data indicate that the final radical pair does show a bleach at 675 nm, which matches the expected wavelength of absorption for P_{D1}. This is considered as the first direct evidence of the secondary donor at the P_{D1} position remaining a chlorophyll-*a* in FR-

PSII. The bandshift on the far-red Chl_{D1} fits well with the steady-state spectra (12) and with what was seen for the $P_{D1}^{+\bullet}Q_A^{-\bullet}$ radical pair spectrum in *Acaryochloris marina* PSII, which is also modelled as a chl-*a* P_{D1} cation with a chl-*d* Chl_{D1} bandshift (34). Therefore, the presence of the electrochromic shift at 725 nm in the nanosecond spectra is strong support for a far-red chlorophyll acting as the primary donor, probably at the Chl_{D1} position (12), and provides additional evidence for the still-contested model that assigns a primary donor role to Chl_{D1} in conventional PSII (3, 4, 15, 7–14).

Although there are signs of the emergence of the 675 nm bleach at 10 ps and 100 ps (Fig. 1a), it is still a minor component in the compartmental spectrum with τ = 720 ps (Fig. 3a) and it is not fully developed until the 2 ns spectra (Fig. 1a,b). The lifetime map (Fig. 1c) indicates an increased bleaching in the 675 nm region at around 60 ps, and then again after 1 ns, which is apparently the lifetime associated with the full development of the bleach. Thus, it appears that the $P_{D1}^{+\bullet}$ is formed later than is generally assumed for WL-PSII which is on the order of a few tens of ps. In fact, the earlier weaker bleach in the 670 nm region may arise from the formation of $Pheo^{-\bullet}$, which is expected to be present in the earlier radical pair(s).

While the $Q_A^{-\bullet}$-induced bandshift on $Pheo_{D1}$ Q_x absorption at 546 nm seemed to be present in the nanosecond spectra, in accordance with low temperature difference spectra (12), this change and that expected from the bleach associated with anion radical formation were not resolved in the ultrafast data (Fig. 3). A possible explanation could be that the electron transfer kinetics are modified in FR-PSII such that transient accumulation is significantly reduced. This kinetic spread could also explain the weakness of the bleach in the Q_y region caused by the presence of $Pheo_{D1}^{-\bullet}$ which is expected in RP1 and RP2.

The excitation energy transfer and charge separation kinetics in FR-PSII might be a manifestation of different sub-populations of centres undergoing charge separation over a range of lifetimes. This would make it more difficult to detect the bleaching and bandshift of the Pheo Q_x band in the spectra at specific delay points. One scenario that could cause such heterogeneity would be the existence of different pathways of excitation energy transfer prior to charge separation. Rapid charge separation would be expected when excitation energy arrives directly at the long-wavelength (~720 nm) primary donor. Slower charge separation would be expected if equilibration between antenna chl-*f* pigments occurs followed by a slower, uphill excitation energy transfer to the 720 nm trap.

It is also worth considering that electron donation from P_{D1} to $Chl_{D1}^{+\bullet}$ may become more favourable by electron transfer from $Pheo^{-\bullet}$ to Q_A since this diminishes the stabilising influence of the adjacent charges on $Chl_{D1}^{+\bullet}Pheo^{-\bullet}$. Thus, the formation of $P_{D1}^{+\bullet}Q_A^{-\bullet}$ as the final radical pair, RP3, may be slow and may not occur as a single discrete electron transfer event. This additional distribution of charge separation kinetics in FR-PSII could also explain the reduced amplitude of the 675 nm bleach associated with the formation of $P_{D1}^{+\bullet}$ in the 2 ns spectra of FR-PSII (Fig. 2) compared to WL-PSII (SI Appendix, Fig. S2b) implying a lower concentration of RP3 state at this time point and a slower rate of formation.

The smaller amount of energy available in FR-PSII appears to modify the steps of charge separation, allowing them to be distinguished. The observation here of the slow $P_{D1}^{+\bullet}$ formation is something that was not possible to detect in WL-PSII because of the overlapping absorption bands of chl-*a* pigments. The possibility exists that this reflects a similar situation occurring in WL-PSII on a faster timescale than in FR-PSII but slower than generally assumed and obscured by spectral overlap.

Materials and Methods

Sample preparation was as described in (12).

White Light PSII (WL-PSII) cores were isolated from *T. elongatus* with His-tagged CP43, and purified by Ni-NTA affinity chromatography essentially as described in (35). Cells were grown in liquid DTN medium at 45°C under white light of 30 µE m^{-2} s^{-1}.

Far-Red Light PSII (FR-PSII) cores were isolated and purified by sucrose density gradient followed by ion exchange chromatography as described in (12). *C. thermalis* PCC 7203 cells were grown in liquid BG11 medium at 30°C under far-red light (750 nm) of 45 µE m^{-2} s^{-1}. All samples were in a buffer of 50 mM MES-NaOH, 5 mM $CaCl_2$, 10 mM $MgCl_2$ and 0.04% (w/v) β-DDM (pH 6.5).

The samples were transferred to a cell (Harrick Scientific, Pleasantville, NY) with 1 mm thickness and 25 mm diameter CaF_2 windows and a 25 µm spacer. The purity of the

sample was assessed by absorption and fluorescence measurements. The absorption spectra for both WL- and FR-PSII samples are presented in the SI Appendix, Fig. S1. The optical density at 675 nm was typically 0.6–0.7. All measurements were performed at room temperature.

Setup

The setup for visible TA measurements was described previously (36). Briefly, the 800 nm output from Ti-Sapphire laser (Spectra Physics, Hurricane, 90 fs, 1 kHz, 0.85 mW) was divided between an optical parametric amplifier (OPA, Spectra Physics, OPA-800C) and a white light generator. The OPA produced three pump wavelengths used in the experiment: 675 nm, 663 nm and 720 nm. The typical bandwidth of the pump radiation was around 20 nm and the energy reaching the sample was below 10 nJ. From the beam diameter of 0.175 mm at the sample position, this energy corresponds to 0.04 W/cm^2 or 42 μJ/cm^2. The delay between the pump and the probe pulses was varied by delaying the pump pulse using a retroreflector mounted on a delay line (M-IMS400CCHA, Newport). Positive delay measurements were subtracted from a background negative delay (-100 ps) measurement representing a 1 ms spectrum with inverted amplitude. The 12 ns and 27 ns measurements were collected by introducing a long delay line using multiple optical mirrors to create additional beam path. To avoid repeated exposure of the same sample volume, the sample was continuously moved in a Lissajous pattern using a home-built sample translator at ST=6 sample translation speed.

The white light was generated using a sapphire plate and spanned the spectral region from 400 to above 800 nm. The probe light was dispersed by a home-built prism spectrometer and registered using 1024 pixel CCD camera at a 1 kHz frame rate on a single-shot basis.

The data were analysed using Global Analysis (23, 37) and Lifetime Density (38, 39) methods. Specifically, freely available Glotaran (40) and the Global analysis toolkit (37) were employed for this purpose. A custom Python code was used for Lifetime Density maps (22). The number of compartments in the results of sequential analysis was chosen based on fitting statistics and residuals.

Acknowledgments

This work was supported by the Leverhulme Trust awards RPG-2014-126 and RPG-2018-372 (to JJvT), BBSRC grants BB/L011506/1, BB/R001383/1 and BB/R00921X/1 (to AWR), a Wolfson Merit Award from the Royal Society (to AWR), and the DFG award NU 421/1-1 (to DJN).

References

1. Cardona T, Murray JW, Rutherford AW (2015) Origin and evolution of water oxidation before the last common ancestor of the cyanobacteria. *Mol Biol Evol* 32(5):1310–1328.

2. Dau H, Zaharieva I (2009) Principles, efficiency, and blueprint character of solar-energy conversion in photosynthetic water oxidation. *Acc Chem Res* 42(12):1861–1870.

3. Rappaport F, Diner BA (2008) Primary photochemistry and energetics leading to the oxidation of the (Mn)4Ca cluster and to the evolution of molecular oxygen in Photosystem II. *Coord Chem Rev* 252(3–4):259–272.

4. Cardona T, Sedoud A, Cox N, Rutherford AW (2012) Charge separation in Photosystem II: A comparative and evolutionary overview. *Biochim Biophys Acta - Bioenerg* 1817(1):26–43.

5. Ferreira KN, Iverson TM, Maghlaoui K, Barber J (2004) Architecture of the Photosynthetic Oxygen-Evolving Center. *Science* 303(5665):1831–1838.

6. Umena Y, Kawakami K, Shen J-R, Kamiya N (2011) Crystal structure of oxygen-evolving photosystem II at a resolution of 1.9 Å. *Nature* 473(7345):55–60.

7. Prokhorenko VI, Holzwarth AR (2000) Primary Processes and Structure of the Photosystem II Reaction Center: A Photon Echo Study. *J Phys Chem B* 104(48):11563–11578.

8. Groot ML, et al. (2005) Initial electron donor and acceptor in isolated Photosystem II reaction centers identified with femtosecond mid-IR spectroscopy. *Proc Natl Acad Sci* 102(37):13087–13092.

9. Holzwarth AR, et al. (2006) Kinetics and mechanism of electron transfer in intact photosystem II and in the isolated reaction center: Pheophytin is the primary electron acceptor. *Proc Natl Acad Sci* 103(18):6895–6900.

10. Diner BA, Rappaport F (2002) Structure, dynamics, and energetics of the primary photochemistry of photosystem II of oxygenic photosynthesis. *Annu Rev Plant Biol* 53(1):551–580.

11. Kawashima K, Ishikita H (2018) Energetic insights into two electron transfer pathways in light-driven energy-converting enzymes. *Chem Sci* 9(17):4083–4092.

12. Nürnberg DJ, et al. (2018) Photochemistry beyond the red limit in chlorophyll f–containing photosystems. *Science* 360(6394):1210–1213.

13. Romero E, Van Stokkum IHM, Novoderezhkin VI, Dekker JP, Van Grondelle R (2010) Two different charge separation pathways in photosystem II. *Biochemistry* 49(20):4300–4307.

14. Romero E, et al. (2012) Mixed exciton-charge-transfer states in photosystem II: Stark spectroscopy on site-directed mutants. *Biophys J* 103(2):185–194.

15. Mamedov M, Govindjee, Nadtochenko V, Semenov A (2015) Primary electron transfer processes in photosynthetic reaction centers from oxygenic organisms. *Photosynth Res* 125(1–2):51–63.

16. Zinth W, Wachtveitl J (2005) The first picoseconds in bacterial photosynthesis - Ultrafast electron transfer for the efficient conversion of light energy. *ChemPhysChem* 6(5):871–880.

17. Miloslavina Y, et al. (2006) Charge separation kinetics in intact photosystem II core particles is trap-limited. A picosecond fluorescence study. *Biochemistry* 45(7):2436–2442.

18. Chen M, et al. (2010) A Red-Shifted Chlorophyll. *Science* 329(5997):1318–1320.

19. Gan F, et al. (2014) Extensive remodeling of a cyanobacterial photosynthetic apparatus in far-red light. *Science* 345(6202):1312–1317.

20. Tomo T, Shinoda T, Chen M, Allakhverdiev SI, Akimoto S (2014) Energy transfer processes in chlorophyll f-containing cyanobacteria using time-resolved fluorescence spectroscopy on intact cells. *Biochim Biophys Acta - Bioenerg*

1837(9):1484–1489.

21. Schmitt FJ, et al. (2018) Photosynthesis supported by a chlorophyll f-dependent, entropy-driven uphill energy transfer in Halomicronema hongdechloris cells adapted to far-red light. *Photosynth Res*:1–17.

22. Dorlhiac GF, Fare C, van Thor JJ (2017) PyLDM - An open source package for lifetime density analysis of time-resolved spectroscopic data. *PLoS Comput Biol* 13(5):e1005528.

23. Van Stokkum IHM, Larsen DS, Van Grondelle R (2004) Global and target analysis of time-resolved spectra. *Biochim Biophys Acta - Bioenerg* 1657(2–3):82–104.

24. Shreve AP, Trautman JK, Frank HA, Owens TG, Albrecht AC (1991) Femtosecond energy-transfer processes in the B800-850 light-harvesting complex of Rhodobacter sphaeroides 2.4.1. *BBA - Bioenerg* 1058(2):280–288.

25. Kleima FJ, et al. (1997) Energy transfer in LHCII monomers at 77K studied by sub-picosecond transient absorption spectroscopy. *Biochemistry* 36(49):15262–15268.

26. Kaucikas M, Nürnberg D, Dorlhiac G, Rutherford AW, van Thor JJ (2017) Femtosecond Visible Transient Absorption Spectroscopy of Chlorophyll f -Containing Photosystem I. *Biophys J* 112:234–249.

27. Zamzam N, Kaucikas M, Nürnberg DJ, Rutherford AW, Van Thor JJ (2019) Femtosecond infrared spectroscopy of chlorophyll f-containing photosystem I. *Phys Chem Chem Phys* 21(3):1224–1234.

28. Nuijs AM, van Gorkom HJ, Plijter JJ, Duysens LNM (1986) Primary-charge separation and excitation of chlorophyll a in photosystem II particles from spinach as studied by picosecond absorbance-difference spectroscopy. *BBA - Bioenerg* 848(2):167–175.

29. Schatz GH, Brock H, Holzwarth AR (1987) Picosecond kinetics of fluorescence and absorbance changes in photosystem II particles excited at low photon density. *Proc Natl Acad Sci U S A* 84(23):8414–8.

30. Pawlowicz NP, Groot M-L, van Stokkum IHM, Breton J, van Grondelle R (2007) Charge separation and energy transfer in the photosystem II core complex studied by femtosecond midinfrared spectroscopy. *Biophys J* 93(8):2732–42.

31. Niedzwiedzki DM, Liu H, Chen M, Blankenship RE (2014) Excited state properties of chlorophyll f in organic solvents at ambient and cryogenic temperatures. *Photosynth Res* 121(1):25–34.

32. Kalaji HM, et al. (2012) Experimental in vivo measurements of light emission in plants: A perspective dedicated to David Walker. *Photosynth Res* 114(2):69–96.

33. Allakhverdiev SI, et al. (2016) Chlorophylls d and f and their role in primary photosynthetic processes of cyanobacteria. *Biochem* 81(3):201–212.

34. Schlodder E, et al. (2007) Both chlorophylls a and d are essential for the photochemistry in photosystem II of the cyanobacteria, Acaryochloris marina. *Biochim Biophys Acta - Bioenerg* 1767(6):589–595.

35. Sugiura M, Inoue Y (1999) Highly purified thermo-stable oxygen-evolving photosystem II core complex from the thermophilic cyanobacterium Synechococcus elongatus having his-tagged CP43. *Plant Cell Physiol* 40(12):1219–1231.

36. Fitzpatrick AE, Lincoln CN, Van Wilderen LJGW, Van Thor JJ (2012) Pump-dump-probe and pump-repump-probe ultrafast spectroscopy resolves cross section of an early ground state intermediate and stimulated emission in the photoreactions of the Pr ground state of the cyanobacterial phytochrome Cph1. *J Phys Chem B* 116(3):1077–1088.

37. van Wilderen LJGW, Lincoln CN, van Thor JJ (2011) Modelling multi-pulse population dynamics from ultrafast spectroscopy. *PLoS One* 6(3):17373.

38. Slavov C, Hartmann H, Wachtveitl J (2015) Implementation and evaluation of data analysis strategies for time-resolved optical spectroscopy. *Anal Chem* 87(4):2328–2336.

39. Croce R, Müller MG, Bassi R, Holzwarth AR (2001) Carotenoid-to-chlorophyll energy transfer in recombinant major light-harvesting complex (LHCII) of higher plants. I. Femtosecond transient absorption measurements. *Biophys J* 80(2):901–915.

40. Snellenburg JJ, Laptenok SP, Seger R, Mullen KM, Stokkum IHM van (2012) Glotaran : A Java -Based Graphical User Interface for the R Package TIMP. *J Stat Softw* 49(3):1–22.

Figures

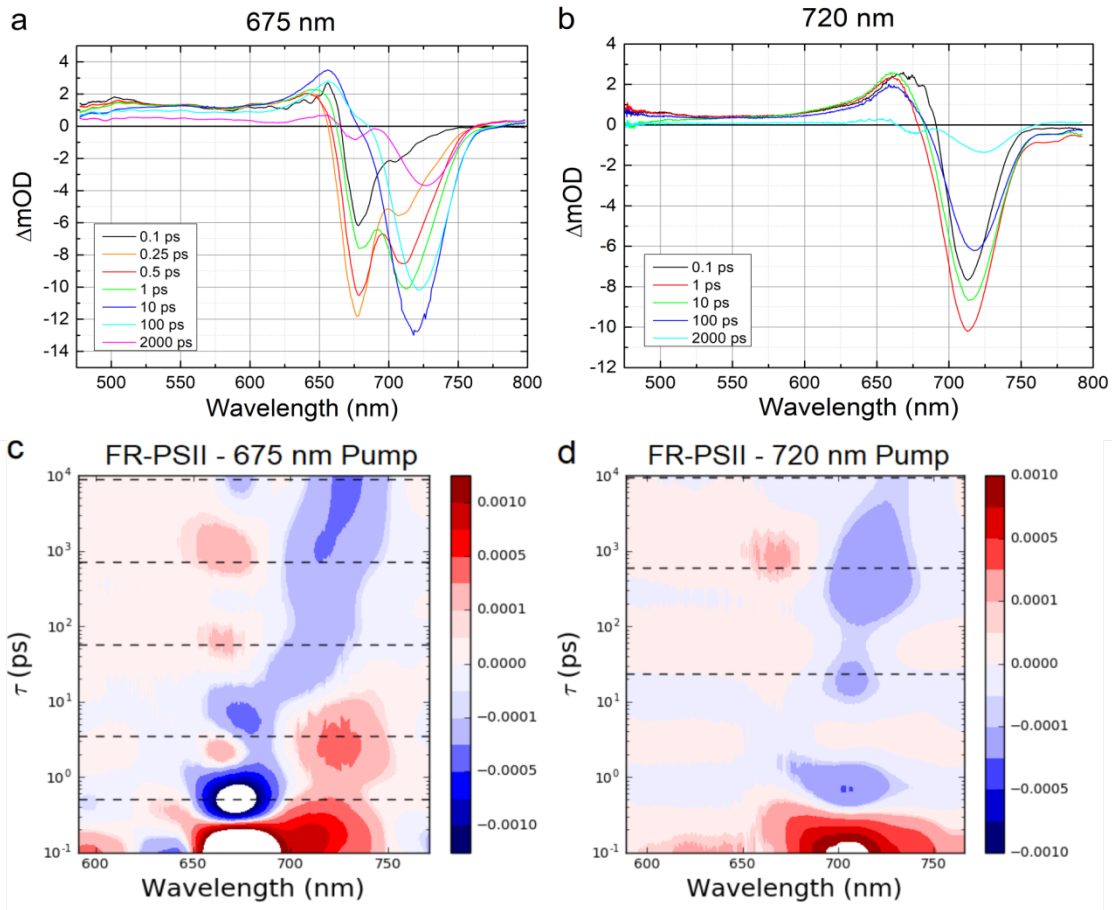

Figure 1. Upper panel: FR-PSII transient absorption spectra at selected delays with (a) 675 nm and (b) 720 nm pump wavelengths. The delay times are between 0.1 ps and 2000 ps as colour coded in the legends. Lower panel: lifetime-density maps of FR-PSII TA data for (c) 675 nm and

(d) 720 nm excitations. Positive amplitudes, represented in red, indicate increased bleaching/stimulated emission or decay of absorption. Negative amplitudes, represented in blue, indicate increased absorption or decay of bleaching/stimulated emission. The dashed lines correspond to the lifetimes associated with the sequential models used to fit the TA data (Fig. 3).

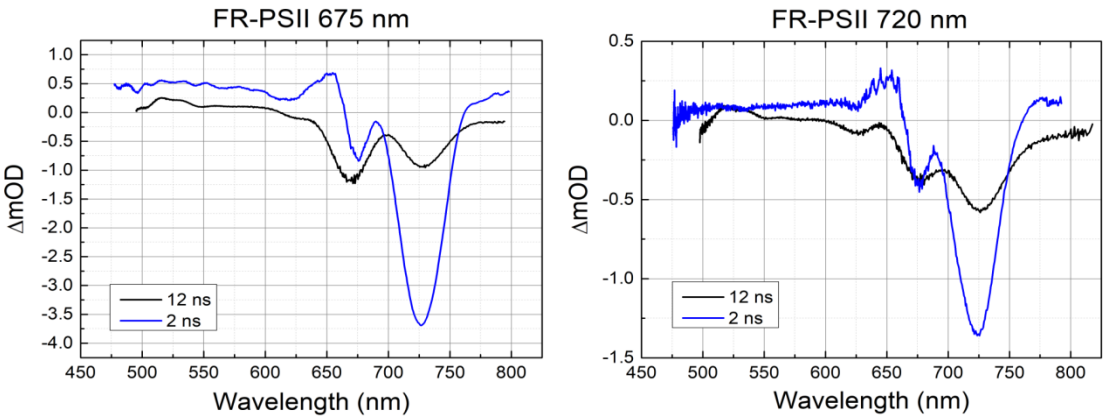

Figure 2. Comparison of 2 ns and 12 ns TA spectra of FR-PSII at 675 nm excitation (left) and 720 nm excitation (right).

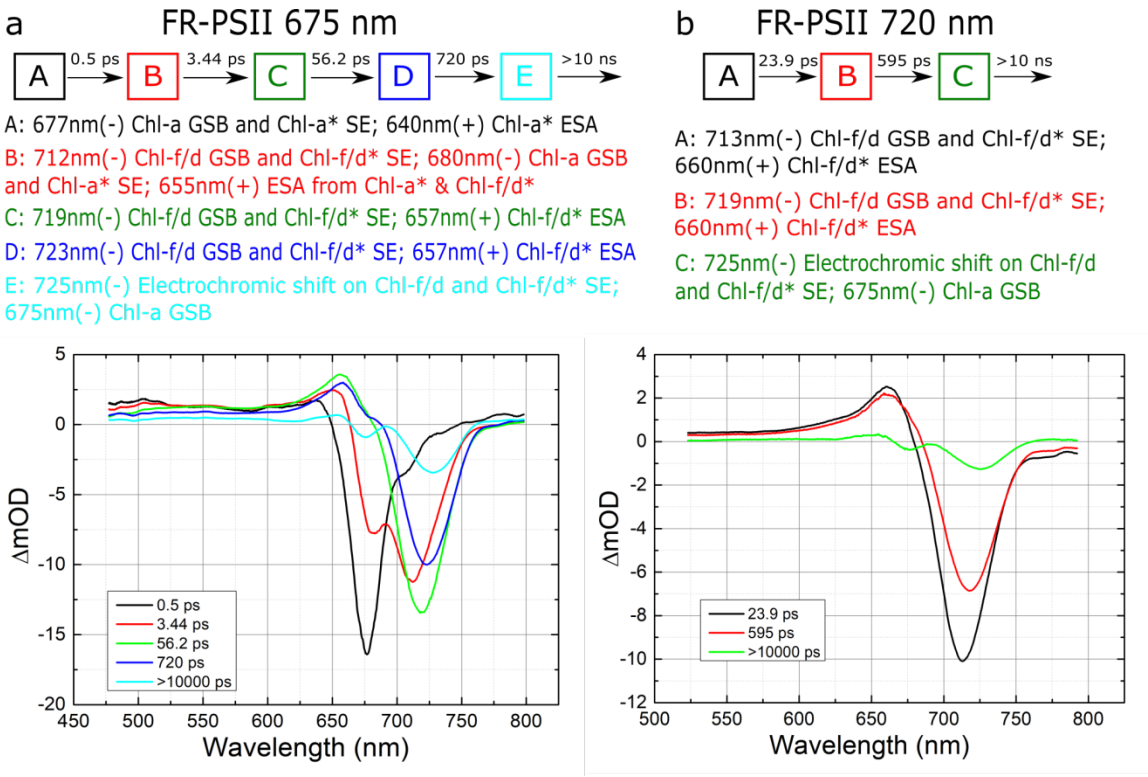

Figure 3. (a) Results of sequential five compartment fit to FR-PSII 675 nm pump data. The time constants are: 0.5 ps, 3.4 ps, 56 ps, 720 ps and >10,000 ps. (b) Results of sequential three compartment fit to FR-PSII 720 nm pump data. The time constants are 23 ps, 595 ps, and >10,000 ps. Above each figure is a representation of the model compartments and a list of the main spectral features with their principle physical assignments in each compartment. Assignments of the features to specific pigments in PSII are suggested in the discussion. GSB: ground state bleach; SE: stimulated emission; ESA: excited state absorption.